

Potassium-Promoted Iron Oxide Model Catalyst Films for the Dehydrogenation of Ethylbenzene: An Example for Complex Model Systems

Guido Ketteler,^{*,†} Wolfgang Ranke,^{*,1} and Robert Schlögl^{*}

^{*}Department Inorganic Chemistry, Fritz-Haber-Institute of the MPG, Faradayweg 4-6, 14195 Berlin, Germany; and [†]FU Berlin, Fachbereich Biologie, Chemie, Pharmazie, Takustr. 3, 14195 Berlin, Germany

Received June 10, 2002; revised August 12, 2002; accepted August 12, 2002

Details of the surface structure and composition of potassium-promoted iron oxide model catalyst films prepared on Ru(0001) are investigated by scanning tunneling microscopy (STM), low-energy electron diffraction (LEED), and Auger electron spectroscopy (AES). At 700 K, polycrystalline KFeO₂ films are formed. On annealing at the temperature of the technical dehydrogenation reaction (870 K), the potassium content in KFeO₂ films decreases and a mixed phase which consists of polycrystalline KFeO₂ on top of partially uncovered K_xFe₂₂O₃₄(0001) forms. Both phases are exposed at the surface. At 970 K, the whole film transforms to K_xFe₂₂O₃₄(0001). Similarities with technical catalyst samples suggest that the pressure gap is bridged, and for the first time, atomic details of the potentially catalytically active surface phase are presented. © 2002 Elsevier Science (USA)

Key Words: potassium; iron oxide; scanning tunneling microscopy; ethylbenzene; dehydrogenation; surface structure; surface phases.

1. INTRODUCTION

Thin oxide films grown on metal substrates have gained much interest as well-defined model catalysts, since they can be prepared with defined stoichiometry and since the conducting substrate enables a detailed characterization by common surface science techniques such as electron spectroscopy and scanning tunnelling microscopy (STM) (1–3). Such films have been prepared for many binary oxides as, for example, Al, Cr, Co, Fe, Ni (1–4). For iron oxides, it has been shown that preparation conditions and electronic structure are comparable to the thermodynamically formed bulk counterparts (5, 6). Recently, even more complex catalyst model systems have been prepared. These include metal particles deposited on oxide supports (7–9), as well as alkali metal-promoted model catalyst films (10–12). The

interaction of potassium with well-defined oxide surfaces has been subject to several investigations (10–18). In combination with catalytic studies, e.g., with a recently developed single-crystal flow reactor (19), one should be able to determine the atomic details and mechanism of catalytic reactions. Potassium-promoted iron oxides are used in the catalytic dehydrogenation of ethylbenzene to styrene in the presence of steam at temperatures of about 870 K (20–22). Recently, we were able to prepare epitaxial potassium-promoted iron oxide model catalyst films by annealing multilayers of potassium deposited on Fe₃O₄(111) at 970 K (10–12). As evidenced by STM and low-energy electron diffraction (LEED) (11), these films have excellent single-crystalline quality, and in combination with X-ray photoelectron spectroscopy (XPS) and thermodynamic considerations (12), we concluded that they consist of single-phase K_xFe₂₂O₃₄(0001). These films can be prepared with varying potassium content giving rise to a (4 × 4), (2 × 2), and (1 × 1) LEED pattern with increasing potassium content (11). XPS measurements showed that around 700 K another ternary potassium iron oxide phase can be prepared which corresponds to KFeO₂ (12). Annealing this phase beyond 870 K leads to a depletion of potassium, establishing a KFeO₂ layer on top of K_xFe₂₂O₃₄(0001) which agrees excellently with investigations of technical catalyst samples (23). Nevertheless, the detailed atomic arrangement of this phase is unknown. All UHV measurements showed that it is difficult to control the potassium content reproducibly, as the residual water gas in an ultra-high vacuum (UHV) environment was found to be highly reactive because it converts the surface of the film to KOH, which desorbs at elevated temperatures. The aim of this study is to get more insight in the preparation, stability, and surface structure of the ternary potassium iron oxide phases forming at 700 K and to reveal details of the surface structure at the technical dehydrogenation temperature of 870 K. The K_xFe₂₂O₃₄(0001) phase, which forms at 970 K, has been previously characterized by STM, LEED, and

¹ To whom correspondence should be addressed. Fax: +49 30 8413 4401. E-mail: ranke@fhi-berlin.mpg.de.

Auger spectroscopy (11) and thus is not addressed in this paper.

2. EXPERIMENTAL

The experiments were performed in an ultrahigh vacuum chamber (UHV) with a base pressure of 1×10^{-10} mbar which is equipped with a scanning tunnelling microscope (STM, Burleigh), a combination of low-energy electron diffraction (LEED) and Auger electron spectroscopy (AES) optics, and oxygen and argon gas inlet valves and a sputter gun. Details are described elsewhere (24). The Ru(0001) substrate single crystal was cleaned by repeated cycles of Ar⁺ sputtering (1 keV, $\sim 3\text{--}5 \mu\text{A}$) and annealing at 1450 K. Iron was evaporated by resistively heating an iron wire wrapped around a tungsten filament. On Ru(0001), closed FeO(111) films with thicknesses of up to 4 ML can be obtained by deposition of the corresponding amount of Fe in one run and subsequent oxidation in 10^{-6} mbar oxygen at 870 K with a final anneal to 970 K (25). On prolonged oxidation, films ≥ 4 ML transform completely into a closed Fe₃O₄(111) film. This offers the opportunity to prepare thin potassium-promoted iron oxide films which allow STM and LEED measurements. Thick films of the K–Fe–O phase forming around 700 K display poor conductivity and the tip approach does not abort, as no tunneling currents can be measured.

Alternatively, hexagonal Fe₃O₄(111) islands can be obtained by a sequence of several iron deposition (submonolayers) and oxidation cycles (26). In this case, the growth is closer to equilibrium conditions, leading to the thermodynamically favored (5) Volmer–Weber growth of Fe₃O₄(111) islands. On prolonged annealing, the Fe₃O₄(111) islands grow at the expense of the surrounding FeO(111) film, which is removed in this way. This is different from Pt(111), where 1- to 2-ML FeO(111) persists, leading to an overall Stranski–Krastanov-like growth mode of iron oxides (27). The Fe₃O₄(111) islands on Ru(0001) have a characteristic hexagonal or triangular shape, and morphology changes of this shape (e.g., facet angles), which might occur on promotion with potassium, may reveal structural information even if no atomic resolution can be achieved.

Potassium was evaporated at room temperature onto closed Fe₃O₄(111) substrate films or on Fe₃O₄(111) islands using a commercial getter source (SAES). The sample was placed about 3 cm from the K source and the pressure did not exceed 5×10^{-9} mbar during deposition. Subsequently, the K/Fe₃O₄(111) films were annealed at 700, 870, and 970 K in vacuum or in 10^{-6} mbar O₂. Auger measurements were carried out at a 3-kV primary beam energy with a modulation voltage of $V_{pp} = 7$ V. STM measurements were performed in the constant current mode using electrochemically etched tungsten tips cleaned *in situ* by electron bombardment.

3. RESULTS

3.1. Characterization of the Fe₃O₄(111) Precursor Films

Fe₃O₄ crystallizes in the inverse spinel structure. Along the (111) axis, oxygen layers alternate with two kinds of iron layers, the so-called kagomé layer and three mix-trigonal layers (Figs. 1a and 1b). Figures 1c and 1d show a LEED pattern and an atomically resolved STM image of a ~ 20 -Å thick Fe₃O₄(111) film grown on Ru(0001) with the 6×6 Å periodicity of the iron layers in this oxide. Additionally, bright features can be seen. Since AES shows only signals from Fe, O, and Ru, we believe that they represent Fe clusters which form because of mass transport during the stoichiometric conversion of closed FeO(111) films to Fe₃O₄(111). LEED and STM images of the films grown on Ru(0001) and Pt(111) look very similar, suggesting that the same surface structure forms on both substrates, which was found by a dynamical LEED analysis to be strongly relaxed and terminated by 1/4 ML of iron cations in the outermost layer (28).

Figure 2a shows the surface morphology of 20- to 40-Å thick, closed Fe₃O₄(111) films. The mesoscopic surface roughness is 30 Å on a length scale of 1 μm, which is in the same range as the roughness of the clean Ru(0001) substrate. Occasionally, hexagonal crystallites with diameters of ~ 1000 Å are formed (marked by the arrows). The step density is low, with terraces several hundred Å wide. Most steps and crystallites are multiples of 4.8 Å high, which corresponds to the repeat unit along (111) and indicates the dominance of one surface termination. Occasionally, lower

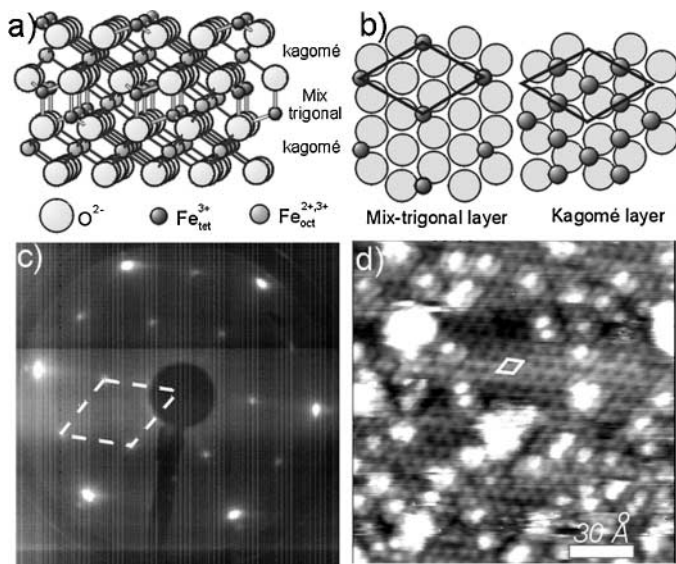


FIG. 1. (a) Slightly tilted side view of Fe₃O₄(111). (b) Top view of the two different iron sublayers of Fe₃O₄(111). (c) LEED pattern (60 eV). (d) $150 \times 150 \text{ \AA}^2$ ($I_t = 0.9 \text{ nA}$, $U_B = +0.7 \text{ V}$) atomic resolution STM image of a ~ 20 -Å thin Fe₃O₄(111) film grown epitaxially on Ru(0001). The unit cell is indicated in the LEED pattern and the STM image.

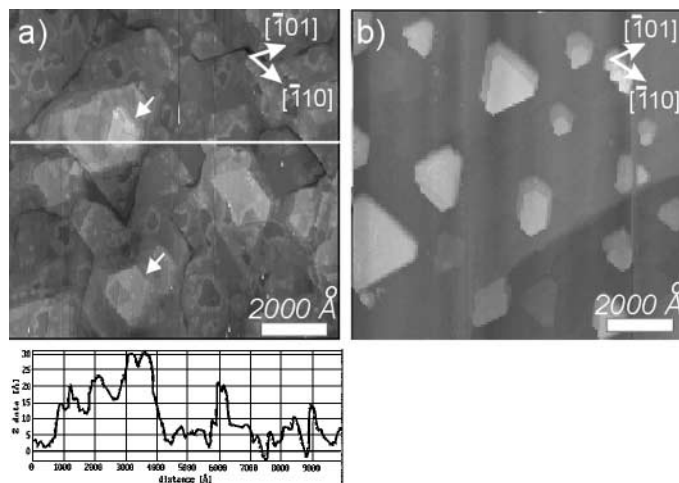


FIG. 2. (a) $1 \times 1 \mu\text{m}^2$ ($I_t = 0.5 \text{ nA}$, $U_B = +1.2 \text{ V}$) large-scale STM image of a $\sim 40\text{-\AA}$ thin $\text{Fe}_3\text{O}_4(111)$ film grown on $\text{Ru}(0001)$. The arrows indicate hexagonal crystallites. (b) $1 \times 1 \mu\text{m}^2$ ($I_t = 1.0 \text{ nA}$, $U_B = +0.1 \text{ V}$) large-scale STM image of $\text{Fe}_3\text{O}_4(111)$ islands grown on $\text{Ru}(0001)$.

step heights are observed. These are due to the formation of “biphase-ordered” $\text{FeO}(111)/\text{Fe}_3\text{O}_4(111)$ domains (29, 30), as also indicated by their characteristic contribution to the LEED pattern (not shown here). As described in Section 2, also $\text{Fe}_3\text{O}_4(111)$ islands can be prepared (Fig. 2b). These crystallites have hexagonal or triangular shape. They are less than 50 \AA high, with diameters between 100 and 3000 \AA .

3.2. Identification of Potassium Iron Oxide Phases

Figure 3 shows the crystal structures of the ternary potassium iron oxides believed to be involved in the dehydrogenation, as deduced from investigations with technical catalyst samples (23). Formation and stability of ternary potassium iron oxides are reviewed in Ref. (12). KFeO_2 and $\text{K}_x\text{Fe}_{22}\text{O}_{34}$ ($x = 2-4$) are the only thermodynamically

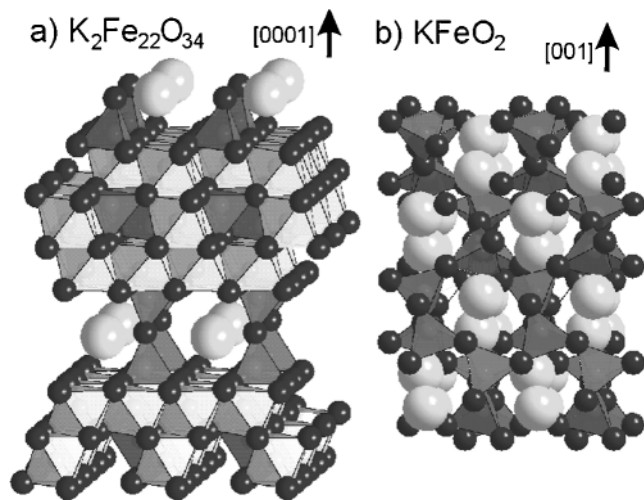


FIG. 3. Structural models for (a) $\text{K}_2\text{Fe}_{22}\text{O}_{34}(0001)$ and (b) KFeO_2 .

stable ternary compounds in the system $\text{K}_2\text{O}-\text{Fe}_2\text{O}_3$, and therefore it is very likely that potassium iron oxides adapt one of these stoichiometries, assuming that the film thickness is sufficient to form the bulk composition. Potassium-poor $\text{K}_x\text{Fe}_{22}\text{O}_{34}$ phases (also called $\text{K}-\beta\text{-Fe}_2\text{O}_3$ ($x = 2$) and $\text{K}-\beta''\text{-Fe}_2\text{O}_3$ ($x = 4$)) exist with varying potassium content (even $x < 2$ has been proposed for isostructural compounds; see references in (12)) and are layered structures consisting of spinel blocks which are very similar to those in $\text{Fe}_3\text{O}_4(111)$. The spinel blocks are separated by KO or K_2O layers. Differences in the stacking of the spinel blocks leads to different lattice constants c (23.8 vs 35.9 \AA), while all structures are hexagonal with $a = b = 5.9 \text{ \AA}$. The potassium-rich KFeO_2 is orthorhombic with lattice constants $a = 5.6 \text{ \AA}$, $b = 11.25 \text{ \AA}$, and $c = 15.9 \text{ \AA}$. The potassium distribution in this phase is much more homogeneous.

Figure 4 shows the evolution of the Auger peak intensity ratios of K/O and Fe/O with time when annealing thin,

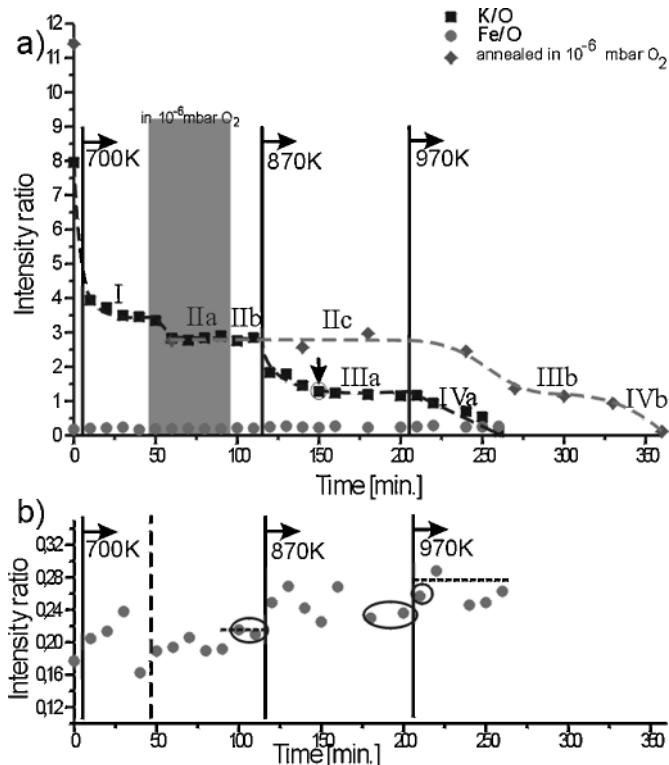


FIG. 4. (a) Evolution of the K/O (squares) and Fe/O (circles) Auger peak intensity ratios with annealing time when annealing $\text{K}/\text{Fe}_3\text{O}_4(111)$ to 700, 870, and 970 K in a vacuum. Annealing in 10^{-6} mbar O_2 is necessary to establish a distinct stoichiometry at 700 K (shaded area). (Diamonds) K/O Auger intensity ratios of a $\text{K}/\text{Fe}_3\text{O}_4(111)$ film which was annealed to 700, 870, and 970 K in a 10^{-6} -mbar oxygen atmosphere. The arrow indicates the intensity ratio of the model catalyst film shown in the STM images in Fig. 8. The different annealing procedures are indicated by the symbols I, IIa–c, IIIa,b, and IVa,b and are explained in the text. (b) Magnification of the Fe/O intensity ratios. Finally, constant Fe/O ratios are attained for the different annealing procedures (circled data points). (Dashed lines) Anticipated Fe/O AES ratios for stoichiometric KFeO_2 (0.213) and $\text{K}_3\text{Fe}_{22}\text{O}_{34}$ (0.276).

closed potassium iron oxide films at different temperatures. K, O, and Fe peaks at energies of 252, 503, and 651 eV, respectively, were chosen to calculate the intensity ratios. For all films, the Ru Auger peaks dominate the spectra, thus indicating very thin films. Annealing at 700 K in vacuum leads to a decrease of the potassium signal until a plateau at $K/O = 3.3$ is reached (Fig. 4, regime I). This value differs depending on the thickness of the $Fe_3O_4(111)$ film and when different amounts of K are deposited. Nevertheless, annealing at 700 K in 10^{-6} mbar O_2 always leads to constant K/O and Fe/O intensity ratios of 2.8 and 0.20, respectively, independent of the $Fe_3O_4(111)$ film thickness and independent of the potassium amount deposited, given that it is above the stoichiometric amount needed to form this phase (Fig. 4, regime IIa). This indicates that the oxygen reservoir of the thin $Fe_3O_4(111)$ films is not sufficient and oxidative conditions are required to form this potassium iron oxide phase. Once this value is attained, annealing in vacuum only slightly increases the Fe/O intensity ratio, to 0.21 (Fig. 4, regime IIb).

Further annealing at 870 K in 10^{-6} mbar O_2 does not change the intensity ratios (Fig. 4, regime IIc). Annealing at the same temperature in vacuum leads to a diminution of the potassium content, and after 50–60 min, constant K/O and Fe/O Auger intensity ratios of 1.0 and 0.24, respectively, are observed (Fig. 4, regime IIIa). These values are close to those observed after annealing very thick films to 970 K (11). As with those films, we observe a weak $Fe_3O_4(111)-(2 \times 2)$ pattern with LEED which was attributed to a $K_xFe_{22}O_{34}(0001)$ phase. The low intensity of the (2×2) LEED pattern may be due to the limited film thickness, which is in the range of the three-dimensional unit cell of the $K_xFe_{22}O_{34}$ (23.8 Å). Further annealing at 970 K leads to a constant decrease of the potassium signal (Fig. 4, regime IVa). In oxygen atmosphere, this decrease is significantly slower and a plateau with a ratio of 1.0 is reached (Fig. 4, regime IIIb) before all potassium desorbs on prolonged annealing (Fig. 4, regime IVb). As potassium depletion occurs preferentially via reaction with residual gas water and desorption of KOH (12), the time axis in Fig. 4 depends on the residual gas pressure.

In summary, the Auger measurements show that two distinct stoichiometries can be obtained. The first one is a potassium-rich phase at 700 K which requires oxidation of the $K/Fe_3O_4(111)$ film. The second phase transition to a compound with lower potassium content depends on the oxygen partial pressure and occurs at 870 K in vacuum or 970 K in 10^{-6} mbar O_2 . The stability ranges agree perfectly with the results from XPS annealing cycles in vacuum and water atmosphere (12), where these equilibrium phases have been attributed to $KFeO_2$ (at 700 K) and $K_xFe_{22}O_{34}$ (above 870 K). Table 1 summarizes the obtained Auger ratios for the identified phases. Only the “ Fe_xO_y ” stoichiometries are calculated from the Auger intensity ratios, as the K distribution in $KFeO_2$ (homogenous) and

TABLE 1

 Auger Peak Intensity Ratios for $Fe_3O_4(111)$ and the Different Potassium Iron Oxide Phases

	$Fe_3O_4(111)$	K/ $Fe_3O_4(111)$		
		700 K	870 K	970 K
$I_K : I_O$	—	2.8	1.0	1.0
$I_{Fe} : I_O$	0.32	0.21	0.24	0.26
Stoichiometry	Fe_3O_4	“ FeO_2 ”	“ $Fe_{19}O_{34}$ ”	“ $Fe_{21}O_{34}$ ”
From XPS (12)	Fe_3O_4	$KFeO_2$	$KFeO_2/K_xFe_{22}O_{34}$	$K_xFe_{22}O_{34}$

Note. The Fe/O stoichiometries are estimated assuming that $I_{Fe}/I_O = 0.32$ corresponds to Fe_3O_4 .

$K_xFe_{22}O_{34}(0001)$ (layered with possible K-rich surface termination) is very different. Fe/O ratios fluctuate strongly before the equilibrium phases are formed but finally attain constant values (encircled data points in Fig. 4b), indicating stoichiometries of “ FeO_2 ” (at 700 K), “ $Fe_{19}O_{34}$ ” (at 870 K), and “ $Fe_{21}O_{34}$ ” (at 970 K). These values are close to the anticipated values for stoichiometric $KFeO_2$ and $K_xFe_{22}O_{34}$ (dashed lines in Fig. 4b).

3.3. Surface Structure of the Low-Temperature Phase ($KFeO_2$)

$KFeO_2$ films prepared by deposition of potassium on thin, closed $Fe_3O_4(111)$ films and annealing at 700 K in 10^{-6} mbar O_2 (regime IIa,b in Fig. 4) display no LEED pattern. STM images are shown in Fig. 5. On a large scale, the mesoscopic surface roughness of the precursor $Fe_3O_4(111)$ film has increased to about 50 Å on a length scale of 6000 Å (Fig. 5a). Terraces several hundred angstroms wide with hexagonally inclined step edges running along the [101]

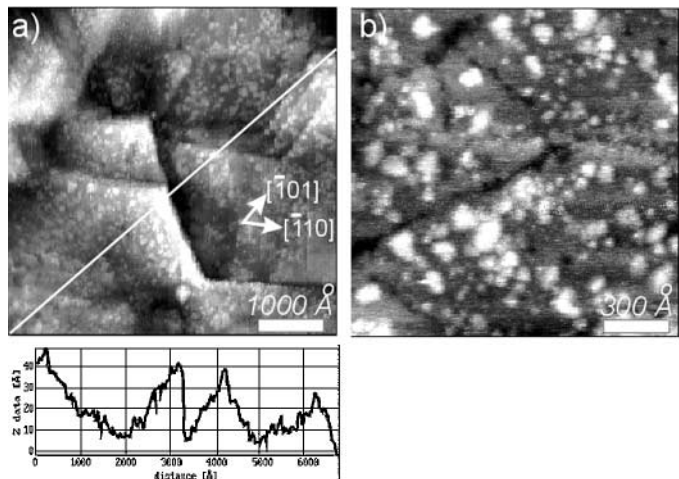


FIG. 5. (a) $5000 \times 5000 \text{ \AA}^2$ ($I_t = 1.0 \text{ nA}$, $U_B = +1.2 \text{ V}$) and (b) $1500 \times 1500 \text{ \AA}^2$ ($I_t = 1.0 \text{ nA}$, $U_B = +1.3 \text{ V}$) STM images of the $KFeO_2$ phase obtained after annealing potassium deposited on $Fe_3O_4(111)$ to 700 K in a vacuum. Crystallographic directions of the $Fe_3O_4(111)$ precursor film are indicated.

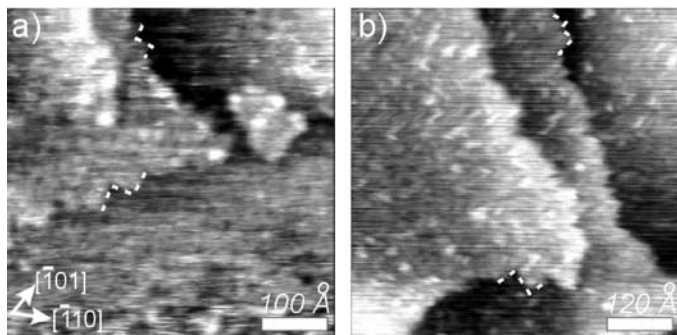


FIG. 6. (a) $500 \times 500 \text{ \AA}^2$ ($I_t = 0.7 \text{ nA}$, $U_B = +2.7 \text{ V}$) and (b) $600 \times 600 \text{ \AA}^2$ ($I_t = 0.7 \text{ nA}$, $U_B = +2.7 \text{ V}$) STM images of the phase obtained after annealing potassium deposited on $\text{Fe}_3\text{O}_4(111)$ to 870 K in a 10^{-6} -mbar oxygen atmosphere. Crystallographic directions of the $\text{Fe}_3\text{O}_4(111)$ precursor film are indicated. These films have the same K/O and Fe/O Auger intensity ratios as the one shown in Fig. 5.

and $[\bar{1}10]$ directions of the precursor $\text{Fe}_3\text{O}_4(111)$ film are observed. The surface morphology thus still is governed by the precursor $\text{Fe}_3\text{O}_4(111)$ film or the Ru(0001) substrate. Closer inspection reveals that the terraces are very rough (Fig. 5b). The film has cracked and is disrupted by several trenches. The terraces are too rough to determine precise step heights.

STM images of a film prepared by oxidation in 10^{-6} mbar oxygen at 870 K (regime IIc in Fig. 4) are shown in Figs. 6a and 6b. Higher bias voltages are now required to resolve this surface. The morphology has changed and apart from 120° or 60° angles, also rectangular step edges are occasionally formed. Also this film displays no LEED pattern.

Experiments with K-promoted $\text{Fe}_3\text{O}_4(111)$ islands reconfirm that the macroscopic morphology of potassium-promoted iron oxides is governed by the precursor $\text{Fe}_3\text{O}_4(111)$ morphology. After promotion with potassium and prolonged annealing at 700 K, triangular or hexagonal islands identical to unpromoted islands are observed (compare Fig. 7a with Fig. 2c). Between the islands, where originally a flat, well-ordered $\text{FeO}(111)$ film existed, new features have formed (Fig. 7b). Flat terraces are now partially covered by a film with a dendritic appearance. Step edges are decorated by this phase as well. The dendritic shape shows that the high dispersion of the $\text{FeO}(111)$ film has vanished, and a sintered phase with an unfavorable epitaxial relationship with respect to the substrate has formed. This agrees well with the alkali-metal-induced sintering observed previously for 1-ML $\text{FeO}(111)$ on Pt(111) (18). The film produces the $\text{Fe}_3\text{O}_4(111)$ LEED pattern superimposed with a Ru(0001)- (3×3) pattern (Fig. 7c). An intense (3×3) LEED pattern is also obtained when potassium is deposited on a clean Ru(0001) substrate without iron oxide present; therefore it does not arise from a new ternary potassium iron oxide phase but results from K/Ru(0001)- (3×3) do-

mains which exist beside the sintered K-Fe-O phase. Annealing at 870 K in 10^{-6} mbar O_2 does not affect the island morphology but the morphology of the regions in between changes (Fig. 7d). Flat terraces are covered by a higher dispersed polycrystalline film. This film is 6–10 Å thick and has similarities to the covering film shown in Fig. 8 (see next section), which can be identified as KFeO_2 . Edges of this phase are in most cases aligned at the Ru(0001) substrate, but no crystalline order is visible. Also here, the K/Ru(0001)- (3×3) LEED pattern is obtained. Experiments with alkali metals on 1-ML $\text{FeO}(111)/\text{Pt}(111)$ showed that prolonged annealing leads to desorption of the alkali metal and as a result the iron oxide spreads back over the Pt(111) (18).

3.4. Surface Structure of Potassium-Promoted Iron Oxides at 870 K

As shown in Section 3.2, annealing a KFeO_2 film at 870 K in a vacuum leads to the formation of a phase with lower potassium concentration. Based on XPS intensity evaluations, this depletion was suggested as proceeding from the bulk under formation of $\text{K}_x\text{Fe}_{22}\text{O}_{34}$ while a potassium-rich

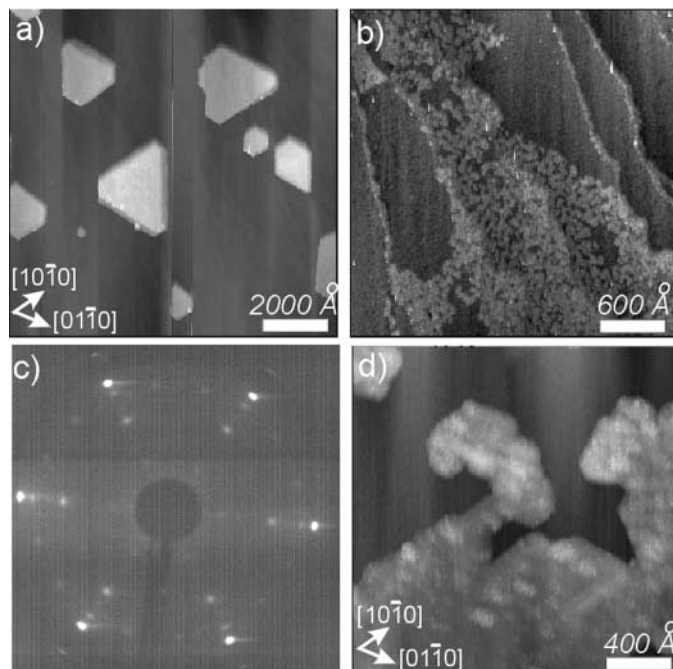


FIG. 7. (a) $1 \times 1 \mu\text{m}^2$ ($I_t = 0.7 \text{ nA}$, $U_B = +1.5 \text{ V}$) large-scale STM image of K deposited on $\text{Fe}_3\text{O}_4(111)$ islands after annealing in a 10^{-6} -mbar oxygen at 700 K. (b) $3000 \times 3000 \text{ \AA}^2$ ($I_t = 0.7 \text{ nA}$, $U_B = +1.5 \text{ V}$) large-scale STM image of the flat regions inbetween the $\text{Fe}_3\text{O}_4(111)$ islands after deposition of K and annealing in 10^{-6} mbar oxygen at 700 K. (c) LEED image (60 eV) of the surface shown in (a) and (b). (d) $2000 \times 2000 \text{ \AA}^2$ ($I_t = 0.8 \text{ nA}$, $U_B = +0.8 \text{ V}$) large-scale STM image after oxidation in 10^{-6} mbar oxygen at 870 K. Crystallographic directions of the Ru(0001) substrate are indicated.

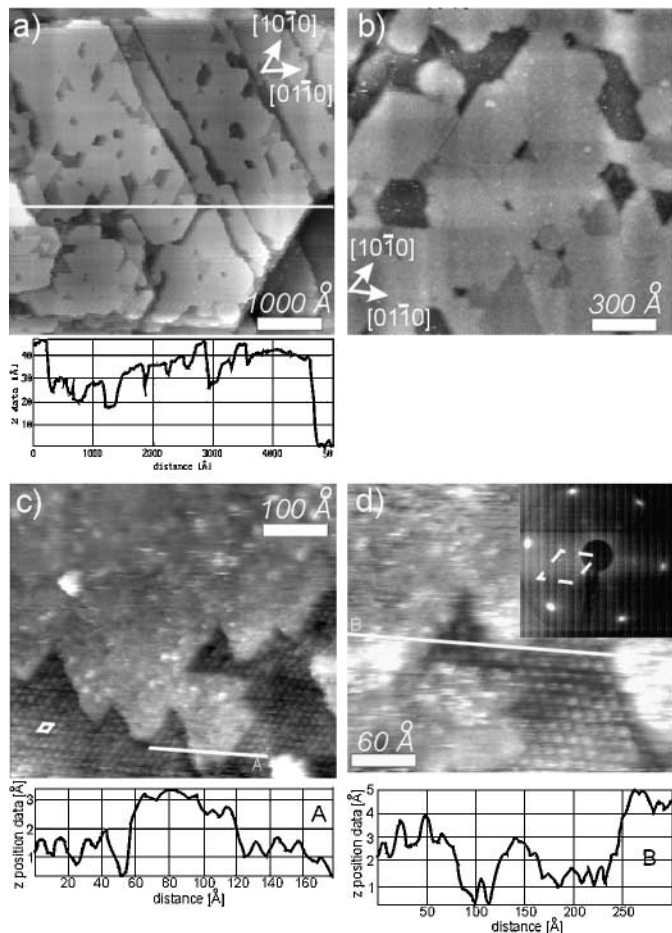


FIG. 8. (a) $5000 \times 5000 \text{ \AA}^2$ ($I_t = 0.8 \text{ nA}$, $U_B = +1.2 \text{ V}$) and (b) $1500 \times 1500 \text{ \AA}^2$ ($I_t = 0.8 \text{ nA}$, $U_B = +1.5 \text{ V}$) large-scale STM images of K deposited on $\text{Fe}_3\text{O}_4(111)$ after annealing for $\sim 35 \text{ min}$ at 870 K . The K/O and Fe/O intensity ratios are indicated by an arrow in Fig. 4. (c) $500 \times 450 \text{ \AA}^2$ ($I_t = 0.2 \text{ nA}$, $U_B = +1.5 \text{ V}$) and (d) $300 \times 265 \text{ \AA}^2$ ($I_t = 0.2 \text{ nA}$, $U_B = +1.5 \text{ V}$) higher resolution STM images with line scans. (Diamonds) The two-dimensional $12 \times 12 \text{ \AA}^2$ unit cell of the $\text{K}_x\text{Fe}_{22}\text{O}_{34}(0001)$ phase. (Inset) The weak (2×2) LEED pattern (13 eV) of the $\text{K}_x\text{Fe}_{22}\text{O}_{34}(0001)$ phase with a lattice constant of $\sim 12 \text{ \AA}$.

KFeO_2 -like surface region is maintained. In order to prepare such a mixed phase, we annealed a KFeO_2 film at 870 K in a vacuum until the constant Auger ratios of the $\text{K}_x\text{Fe}_{22}\text{O}_{34}$ phase were nearly attained (indicated by the arrow in Fig. 4). The characteristic morphology of this film is shown in Figs. 8a and b. The mesoscopic surface roughness is 50 \AA on a length scale of 5000 \AA . The step density is very low and terraces are $500\text{--}2000 \text{ \AA}$ wide. Most step heights are multiples of $\sim 5 \text{ \AA}$. The terraces have hexagonally shaped depressions with diameters of $100\text{--}400 \text{ \AA}$. The two height levels correspond to two different phases which are separated by steps which are $2\text{--}5 \text{ \AA}$ high. The lower regions are very flat and cover about 15% of the surface. Higher resolution STM images reveal a single-crystalline phase with a $12 \times 12 \text{ \AA}$ periodicity (Figs. 8c and 8d). The $12 \times 12 \text{ \AA}$ peri-

odicity is also displayed in the LEED pattern (Fig. 8d, inset) and is well known from $\text{K}_x\text{Fe}_{22}\text{O}_{34}(0001)$ films on $\text{Pt}(111)$ (10, 11). The upper terraces cover about 85% of the surface and have a morphology similar to the KFeO_2 phase (compare Figs. 5 and 6). This phase is in most cases aligned to the crystallographic directions of the $\text{K}_x\text{Fe}_{22}\text{O}_{34}(0001)$ phase but no crystalline order is visible. Further annealing causes this KFeO_2 phase to disappear. The remaining well-ordered $\text{K}_x\text{Fe}_{22}\text{O}_{34}(0001)$ surface was investigated in (11).

4. DISCUSSION

The Auger measurements indicate the formation of two different distinct stoichiometric compounds when potassium is deposited on $\text{Fe}_3\text{O}_4(111)$ and annealed to different temperatures. The stoichiometries deduced from AES for both phases (Table 1) as well as the characteristic temperatures of formation agree perfectly with previous XPS investigations and thermodynamic considerations (12). The first phase corresponds to polycrystalline or amorphous KFeO_2 . These KFeO_2 films on $\text{Ru}(0001)$ could not be prepared in single-crystalline quality since annealing at temperatures beyond 870 K leads to formation of other ternary phases ($\text{K}_x\text{Fe}_{22}\text{O}_{34}(0001)$) or desorption of potassium. Even after prolonged annealing for several hours at 700 or at 870 K in oxygen atmosphere, we could not observe a defined LEED pattern of this phase. STM images obtained under these two conditions are quite similar. In general, films annealed at 870 K in oxygen are less corrugated in large-scale images and require higher bias voltages for tunneling. This indicates that these films have fewer defects, which according to the differences in the preparation are very likely oxygen vacancies. This would explain the higher bias voltages necessary to tunnel oxygen-annealed films. Nevertheless, the K/O and Fe/O Auger intensity ratio is not significantly different for both conditions; thus differences in the oxide stoichiometry are quite small. On a small scale, both films show rough terraces without long-range order. No atomic resolution was obtained with STM, which may be due to the high bias voltages and to the roughness of the film. In some cases, hexagonal as well as right angles are observed at step edges. The latter may indicate that the material is of a space group with right angles (e.g., orthorhombic KFeO_2).

As we have shown above, it makes a difference whether KFeO_2 films are annealed in a vacuum or in an oxygen atmosphere: At 870 K , depletion of potassium and transformation into $\text{K}_x\text{Fe}_{22}\text{O}_{34}(0001)$ was only observed in vacuum while in oxygen atmosphere KFeO_2 remained stable, which simply indicates that the stability ranges of the involved oxides depend on temperature and oxygen partial pressure. The catalytic dehydrogenation of ethylbenzene is performed at 870 K , and we observe a depletion of potassium at

this temperature which finally leads to the single-crystalline $K_xFe_{22}O_{34}(0001)$ phase. Slightly before the constant Auger ratio of this phase is reached, most of the film is still covered with polycrystalline $KFeO_2$. Only small sections of $K_xFe_{22}O_{34}(0001)$ can be seen in large-scale STM images (Fig. 8). Nevertheless, as the Auger ratio is already very close to the value of the pure $K_xFe_{22}O_{34}(0001)$ phase, we can conclude that a thin $KFeO_2$ film has formed on top of $K_xFe_{22}O_{34}(0001)$ instead of thick $KFeO_2$ domains. This confirms the proposition deduced from XPS, that the depletion of the film goes along with a decrease in the potassium content in the bulk while the surface remains potassium rich (12). Both phases are exposed side by side at the surface. These films therefore appear to model the catalytically active phase quite well, which according to investigations of the technical catalyst consists of a $KFeO_2$ shell forming around a core of $K_2Fe_{22}O_{34}$.

The technical dehydrogenation of ethylbenzene is performed in an excess of steam. Water may have two different functions. It may have an oxidizing impact due to the liberation of oxygen by thermal decomposition into hydrogen and oxygen at high temperatures. According to the dissociation equilibrium, the partial pressures of O_2 and H_2 for 1 bar H_2O at 870 K are 6.4×10^{-6} and 1.3×10^{-5} mbar, respectively (5). The oxidizing or reducing impact of water would thus be close to UHV conditions. On the other hand, water may react with the potassium iron oxides under formation of KOH, which at this temperature has a considerable vapor pressure and may desorb. Previous XPS experiments showed that the phase transition to $KFeO_2$ and $KFe_{22}O_{34}(0001)$ occurred at the same temperatures in a vacuum and in a 10^{-8} -mbar H_2O water atmosphere (12); therefore the mixed $KFeO_2/KFe_{22}O_{34}(0001)$ surface structure shown here may also form at 870 K in water atmosphere. However, formation of the K-rich $KFeO_2$ surface phase then competes with K removal by KOH formation and desorption, and its existence therefore depends on its rate of formation. As the technical catalyst was identified to consist of $KFeO_2$ and $KFe_{22}O_{34}$ (21, 23), the removal of potassium by KOH desorption has to be compensated for in a dynamic process in which potassium segregates from the underlying $KFe_{22}O_{34}$ phase to the surface. In this way, the $KFe_{22}O_{34}$ phase serves as a potassium reservoir for the recovery of the $KFeO_2$ surface phase. The required potassium diffusion is a very fast process. This is evident from XPS measurements which showed that at 300 K a solid-state reaction occurs and KO_2 is formed by reaction with oxygen from the $Fe_3O_4(111)$ substrate (12). Presently, it is not clear how the complete removal of potassium from the catalyst in its active state by formation and desorption of KOH is avoided under real catalysis conditions. The deactivation of the catalyst by spatial disintegration into Fe_3O_4 and bulk KOH is a slow process (21, 23), and it is likely that carbonaceous deposits serve as a protective layer against K depletion (22).

5. CONCLUSIONS

Using STM and AES, we investigated the stability ranges of potassium-promoted iron oxide model catalyst films in dependence on the annealing temperature and oxygen partial pressure. In agreement with the stability ranges of potassium-promoted iron oxide model catalyst films prepared on a Pt(111) substrate, we found that the same $KFeO_2$ phase forms at 700 K, while at higher temperatures single-crystalline $K_xFe_{22}O_{34}(0001)$ becomes more stable. We see no effect of the substrate on the stoichiometry or crystalline quality of the model catalyst film. The Ru(0001) substrate enables the growth of thinner closed films than on Pt(111), leading to sufficient conductivity of the insulating $KFeO_2$ film to image this surface with STM. At conditions which simulate the technical dehydrogenation reaction, $K_xFe_{22}O_{34}(0001)$ is partially covered by $KFeO_2$. Both phases are exposed at the surface. As the same $KFeO_2$ shell around a $K_2Fe_{22}O_{34}$ core was identified for the active state in technical catalyst samples (23), our results hint that the pressure and material gap might be bridged for the experiments shown here, and for the first time, details of the surface of the potentially catalytically active phase are presented.

ACKNOWLEDGMENT

The authors thank Thomas Bunke for experimental assistance.

REFERENCES

- Street, S. C., Xu, C., and Goodman, D. W., *Annu. Rev. Phys. Chem.* **48**, 43 (1997).
- Freund, H.-J., *Angew. Chem.* **109**(5), 444 (1997).
- Noguera, C., *J. Phys. Condens. Matter* **12**, R367 (2000), and references therein.
- Weiss, W., and Ranke, W., *Prog. Surf. Sci.* **70**, 1 (2002).
- Ketteler, G., Weiss, W., Ranke, W., and Schlögl, R., *Phys. Chem. Chem. Phys.* **3**, 1114 (2001).
- Schedel-Niedrig, Th., Weiss, W., and Schlögl, R., *Phys. Rev. B* **52**, 17449 (1995).
- Bäumer, M., and Freund, H.-J., *Prog. Surf. Sci.* **61**, 127 (1999).
- Cosandey, F., and Madey, T. E., *Surf. Rev. Lett.* **8**, 73 (2001).
- Chusuei, C. C., Lai, X., Luo, K., and Goodman, D. W., *Top. Catal.* **14**, 71 (2001).
- Shaikhutdinov, Sh. K., Joseph, Y., Kuhrs, C., Ranke, W., and Weiss, W., *Faraday Discuss.* **114**, 363 (1999).
- Shaikhutdinov, Sh. K., Weiss, W., and Schlögl, R., *Appl. Surf. Sci.* **161**, 497 (2000).
- Joseph, Y., Ketteler, G., Kuhrs, C., Ranke, W., Weiss, W., and Schlögl, R., *Phys. Chem. Chem. Phys.* **3**, 4141 (2001).
- Campbell, C. T., *Surf. Sci. Rep.* **27**, 1 (1997).
- Murray, P. W., Condon, N. G., and Thornton, G., *Surf. Sci. Lett.* **323**, L281 (1995).
- Huang, H. H., Jiang, X., Zou, Z., Chin, W. S., Xu, G. Q., Dai, W. L., Fan, K. N., and Deng, J. F., *Surf. Sci.* **412/413**, 555 (1998).
- Carley, A. F., Jackson, S. D., Roberts, M. W., and O'Shea, J., *Surf. Sci.* **454**, 141 (2000).

17. Nerlov, J., Hoffmann, S. V., Shimomura, M., and Møller, P., *Surf. Sci.* **401**, 56 (1998).
18. Vurens, G. H., Strongin, D. R., Salmeron, M., and Somorjai, G. A., *Surf. Sci. Lett.* **199**, L387 (1988).
19. Kuhrs, C., Swoboda, M., and Weiss, W., *Top. Catal.* **15**, 13 (2001).
20. Geus, J. W., *Appl. Catal.* **25**, 313 (1986).
21. Muhler, M., Schlögl, R., and Ertl, G., *J. Catal.* **138**, 413 (1992).
22. Kuhrs, C., Arita, Y., Weiss, W., Ranke, W., and Schlögl, R., *Top. Catal.* **14**, 111 (2001).
23. Muhler, M., Schütze, J., Wesemann, M., Rayment, T., Dent, A., Schlögl, R., and Ertl, G., *J. Catal.* **126**, 339 (1990).
24. Weiss, W., Ritter, M., Zscherpel, D., Swoboda, M., and Schlögl, R., *J. Vac. Sci. Technol. A* **16**, 21 (1998).
25. Ketteler, G., and Ranke, W., *Phys. Rev. B* **66**, 033405 (2002).
26. Ketteler, G., and Ranke, W., manuscript in preparation.
27. Weiss, W., and Ritter, M., *Phys. Rev. B* **59**, 5201 (1999).
28. Ritter, M., and Weiss, W., *Surf. Sci.* **432**, 81 (1999).
29. Condon, N. G., Leibsle, F. M., Parker, T., Lennie, A. R., Vaughan, D. J., and Thornton, G., *Phys. Rev. B* **55**, 15885 (1997).
30. Shaikhutdinov, Sh. K., Ritter, M., Wang, X.-G., Over, H., and Weiss, W., *Phys. Rev. B* **60**, 11062 (1999).